https://doi.org/10.5194/egusphere-2023-2315
Preprint. Discussion started: 26 October 2023

Measurement report: Shipborne observations of black carbon aerosols in the western Arctic Ocean during summer and autumn 2016–2020: boreal fire impacts

Yange Deng[1], Hiroshi Tanimoto[1], Kohei Ikeda[1], Sohiko Kameyama[2], Sachiko Okamoto[1,a], Jinyoung Jung[3], Young Jun Yoon[3], Eun Jin Yang[3] and Sung-Ho Kang[3]

1 National Institute for Environmental Studies, Tsukuba, Japan

2 Hokkaido University, Sapporo, Japan

3 Korea Polar Research Institute, Incheon, Korea

a now at: University Paris Est Creteil and Université de Paris Cité, CNRS, LISA, 94010 Créteil, France

Correspondence to: Hiroshi Tanimoto (tanimoto@nies.go.jp)

Black carbon (BC) aerosol is considered one of the important contributors to the fast climate warming and snow and sea ice melting in the Arctic. Yet the observations of BC in the Arctic Ocean have been limited due to infrastructural and logistical difficulties. We observed BC mass concentrations (m_{BC}) using light absorption methods on board the icebreaker R/V *Araon* in the Arctic Ocean (166° E–156° W and <80° N) as well as the North Pacific Ocean in summer and early Autumn of 2016 to 2020. The levels, interannual variations and pollution episodes of m_{BC} in the Arctic were examined, and the emission sources responsible for the high-BC episodes were analyzed with global chemistry-transport model simulations. The average m_{BC} in the surface air over the Arctic Ocean (72–80° N) observed in 2019 was over 70 ng m^{-3}, which was substantially higher than in other years (approximately 10 ng m^{-3}). The much higher m_{BC} observed in 2019 was perhaps due to more frequent wildfires occurred in the Arctic region than in other years. The model suggested that biomass burning composed the largest contribution to the observed BC in the western Arctic Ocean and the marginal seas. For these five years, we identified 10 elevated-BC episodes, including one in 2018 that was associated with co-enhancements of CO and CH_4 but not CO_2 and O_3. The model analysis indicated that most episodes were attributed to the airmasses transported from boreal fires to the Arctic Ocean, with some near-surface and others in the mid-troposphere. This study provides crucial datasets on BC mass concentrations and the mixing ratios of O_3, CH_4, CO, and CO_2 in the western Arctic Ocean regions and highlights the significant impact of boreal fires on the observed Arctic BC during the summer and early autumn months.

https://doi.org/10.5194/egusphere-2023-2315
Preprint. Discussion started: 26 October 2023

1 Introduction

The climate warming rate in the Arctic is more than three times of the global average, resulting in a rapid decline of Arctic sea ice and extreme cold events, and other ecosystem changes (AMAP, 2021b; IPCC, 2021). While global anthropogenic carbon dioxide (CO_2) emissions play the dominant role in driving Arctic climate change, short-lived climate forcers (SLCFs) – such as methane (CH_4), ozone (O_3), nitrogen oxides, and aerosols – has considerable potential to mitigate climate warming in the Arctic (AMAP, 2015). Aerosol chemical composition can include black carbon (BC), sulphate (SO_4), nitrate (NO_3), organics, sea-salt, and mineral dust. Particularly, BC aerosols in the Arctic atmosphere can absorb solar radiation directly which causes direct/semi-direct climate forcing and work as cloud condensation nuclei (CCN) which causes indirect climate forcing (McFarquhar et al., 2011). When deposited onto snow/ice surface, BC can also affect the radiation due to reduction of the surface albedo; besides, it can accelerate the snow/ice melting due to its light absorption ability. According to Oshima et al. (2020), BC in the Arctic provides the second largest contribution to the positive effective radiative forcings after CO_2. Therefore, BC plays an important role in Arctic climate forcing.

Systematic monitoring of BC in the Arctic is warranted to provide a better scientific basis for making mitigation policies. Long-term BC observations have been carried out in observatories on continental Arctic, such as Barrow/Utqiaġvik, Alert, Zeppelin, Summit, Pallas and Tiksi, and Gruvebadet (Stohl et al., 2013; Schmale et al., 2022). Whereas those data provided essential information on the seasonal and interannual variations of BC in the Arctic (e.g., Schmale et al., 2022), they are limited in representing the spatial variation of BC in the Arctic Ocean. Such limitations can be partially compensated for by shipborne and airborne observations. Airborne observations, especially aircraft-based ones, are less constrained from earth-surface conditions and allow the vertical profiles of BC in different seasons to be evaluated (e.g., Schulz et al., 2019; Ohata et al., 2021a; Jurányi et al., 2023). Shipborne observations allow for in situ measurements in the remote Arctic Ocean especially in summer and autumn when the Arctic sea ice is at the minimum (Xie et al., 2007; Sierau et al., 2014; Kim et al., 2015; Sakerin et al., 2015, 2021; Taketani et al., 2016, 2022; Popovicheva et al., 2017; Ding et al., 2018; Terpugova et al., 2018; Shevchenko et al., 2019; Pankratova et al., 2020; Park et al., 2020; Nagovitsyna et al., 2023). In addition, Boyer et al. (2023) measured the BC mass concentration over the central Arctic (>80° N) for a whole year from September 2019 to October 2020. These shipborne studies have provided preliminary results of BC mass concentrations for model evaluation in the Arctic Seas (e.g., Whaley et al., 2022). They also revealed important characteristics of the spatial distribution of BC in the Arctic Ocean and its marginal seas such as the BC concentration decreases with the growing distance from the source region (Xie et al., 2007; Sakerin et al., 2015, 2021). The year-round observation in the central Arctic by Boyer et al. (2023) indicated that

https://doi.org/10.5194/egusphere-2023-2315
Preprint. Discussion started: 26 October 2023

seasonal changes in BC are similar to those of the Arctic continent, but relatively large, with high values in winter and low values in summer. However, most of those studies limited to the North Atlantic and Eurasian Arctic Seas (Sierau et al., 2014; Sakerin et al., 2015, 2021; Popovicheva et al., 2017; Terpugova et al., 2018; Shevchenko et al., 2019; Pankratova et al., 2020; Nagovitsyna et al., 2023; Boyer et al., 2023) and the close to land Bering, Chukchi, and Beaufort Seas (Xie et al., 2007; Kim et al., 2015; Sakerin et al., 2015; Taketani et al., 2016, 2022; Ding et al., 2018; Nagovitsyna et al., 2023). To our knowledge, Xie et al. (2007) and Ding et al. (2018) are the only two studies that reported BC observations in the western Arctic Ocean north of 74° N, and Shevchenko et al. (2019) is the only study related to BC observation in the East Siberian Sea. Furthermore, BC in Xie et al. (2007) was only qualitatively quantified. Therefore, for a better understanding of the spatial-temporal variations of BC in the Arctic Ocean and better model constraint, continuous shipborne observations of BC in the Arctic marine boundary layer especially in the western central Arctic Ocean and East Siberian Sea are highly necessary under the rapidly changing Arctic environments (AMAP, 2021b; Whaley et al., 2022; Jurányi et al., 2023).

The accurate location of BC sources is another important step toward mitigation measures. Atmospheric modelling is indispensable in understanding the distributions and sources of BC in the Arctic quantitatively. Whereas models have been improving in the past two decades, current atmospheric models still have difficulties in accurately reproducing the BC abundance in the Arctic (e.g., Whaley et al., 2022; Jurányi et al., 2023). The main obstacles include poor understanding in long-range transport, vertical mixing, deposition, and emissions (e.g., Ikeda et al., 2017; Whaley et al., 2022). Preexisting modeling studies combined with field observations indicate that biomass burning from Siberia as well as Alaska and Canada contributed the most to surface BC mass concentration during summer and early autumn (e.g., Zhu et al., 2020; Popovicheva et al., 2022). In addition, according to McCarty et al. (2021), wildfire emissions of BC above 60° N have increased from 2010 to 2020 and open biomass burning contributed 56 % of BC emissions above 65° N in 2020. In the context of climate change, the likelihood of extreme Arctic fire weather will increase. Consequently, the impact of BC emissions from boreal vegetation fires on the Arctic atmospheric BC may increase (AMAP, 2021a, b). Therefore, continual studies combining field observations and modelling simulations on the impact and transport of biomass burning BC in boreal areas to the Arctic Ocean is urgently needed.

In this study, BC monitors based on light absorption theory were operated during the 2016–2020 summer and autumn expeditions from the North Pacific Ocean to the Arctic Ocean, encompassing the western Arctic Ocean and part of the east Siberian Sea, and back to the North Pacific Ocean to measure the BC mass concentration (m_{BC}). Based on the observations, the spatial-temporal variations of m_{BC} were characterized and the background m_{BC} in the western Arctic Ocean was derived. The observations were compared with

https://doi.org/10.5194/egusphere-2023-2315
Preprint. Discussion started: 26 October 2023

BC tagged-tracer simulations using GEOS-Chem (Ikeda et al., 2017). The sources of observed BC and air masses containing high BC mass concentrations were interpreted based on GEOS-Chem model and back trajectory analysis. The results from this study demonstrate the significant impacts of boreal fires on the observed BC in the western Arctic Ocean and its marginal seas.

2 Shipborne observations

The shipborne observations were conducted in summer and autumn in the years of 2016 to 2020 (Fig. S1a) on board the icebreaker R/V *Araon* operated by the Korea Polar Research Institute (KOPRI), South Korea. The air intake was set at the handrail of the front upper deck to avoid ship exhaust pollution. A cyclone was attached at the intake to selectively sample $PM_{2.5}$ aerosols. The total air flow rate was 10 L/min.

A continuous soot monitoring system (COSMOS, model 3130, KANOMAX, Japan) and an Aethalometer (model AE33, Magee Scientific Co., USA) were used in the cruises in 2016–2019 and in 2020, respectively, to measure the mass concentrations of BC aerosols. Both instruments use light absorption methods. Therefore, the obtained mass concentration of BC is equivalent black carbon (eBC, Petzold et al., 2013). Nonetheless, BC will be used throughout the manuscript if not specifically mentioned. COSMOS monitors changes in transmittance of 565 nm wavelength LED light across an automatically advancing quartz fiber filter tape. To achieve measurements with high sensitivity and a lower detectable light absorption coefficient, COSMOS uses a double-convex lens and optical bundle pipes to maintain high light intensity and signal data are obtained at 1000 Hz. The data integration time was set to 1 min, which was then averaged to 1 h for further analysis. In addition, its sampling flow rate (0.9 L min^{-1}) and optical unit temperature were actively controlled. The inlet line for COSMOS was heated to 400 °C to effectively volatilize non-refractory aerosol components that were internally mixed with BC. The lowest detection limit of COSMOS at 1 min time resolution is 50 ng m^{-3} and at 1 h time resolution is 1 ng m^{-3} (Ohata et al., 2019). Aethalometer uses the absorption of light at a wavelength of 880 nm by the ambient aerosols collected on a Pallflex Teflon-coated glass fiber (TFE) filter tape to determine the BC concentration. The flow rate was set to 5 L min^{-1}. The data integration time was set to 5 min, which was then averaged to 1 h for further analysis. The default mass absorption cross section value of 7.77 m^2 g^{-1} and internal multiple scattering correction factor of 1.57 were applied (Drinovec et al., 2015). The lower detection limit of Aethalometer at 1 h time resolution is 5 ng m^{-3}. It is noted that the default parameter settings of the aethalometer may cause the obtained BC mass concentrations to be twice the actual values (Laing et al., 2020; Asmi et al., 2021).

In addition, the atmospheric mixing ratios of CH_4, carbon monoxide (CO), and CO_2 were monitored using a cavity ring-down spectrometer (CRDS) - the Picarro G2401 gas concentration analyzer (Picarro, Inc., USA) when the icebreaker R/V *Araon* was in the Arctic Ocean (North of 72° N) during the cruise in 2018.

https://doi.org/10.5194/egusphere-2023-2315
Preprint. Discussion started: 26 October 2023

The Picarro G2401 analyzer was calibrated by running the standard CH_4 gas (RIGAS, Korea) for 8 min every day. The CH_4, CO, and CO_2 data during the instrument calibration period were omitted. The CH_4, CO, and CO_2 data were averaged to 1 min before being further analyzed. The mixing ratios of O_3 were determined using ultraviolet absorption spectroscopy during the cruises in 2017 and 2018 with a time resolution of 1 min. The O_3 monitor (Model 1100, Dylec Inc., Japan) utilized absorption at 253.7 nm emitted by a low-pressure mercury lump and was calibrated through intercomparison with a reference photometer, which was referenced to the Standard Reference Photometer (SRP) #2 at the National Institute of Standards and Technology (NIST). Those gaseous data were used to assist the analysis on BC sources during high BC episodes in 2018 (Sect. 4.4.2). The O_3 data were also used to scrutinize the possible contamination from ship emissions as explained in the next paragraph. Statistics of those gaseous data are shown in Appendix Table A1; times series and concentration distributions of those data along the cruise tracks are presented in Figs. 6-8 and S14.

To avoid the influence of ship exhausts, we only used 1- or 5-min data records that occurred when the 1-min wind direction and speed relative to the ship's course were within ±60° of the bow and >3 m s^{-1}, respectively, for continuous 10 min centered around the current 1- or 5-min data record. Furthermore, for the 2017 and 2018 cruise, when the atmospheric mixing ratio of O_3 were recorded (Fig. S14), BC and O_3 data were further scrutinized for the possible contamination of ship exhausts considering the O_3 titration effect by NO from ship emissions (Pfannerstill et al., 2019). When O_3 decreased and BC increased at the same time, both 1-min BC and O_3 data were considered invalid. Accordingly, 41–57 % of the observed 1- or 5-min BC data, 56 % of 1-min O_3 data, and 63 % of 1-min CH_4, CO, and CO_2 data were removed from the analysis. Furthermore, hourly values are only calculated when there are more than 40 minutes of valid data records in an hour, by averaging the 1-min or 5-min values within that hour.

3 Model simulations

Tagged tracer simulations of BC using the global chemistry transport model GEOS-Chem (v13.1.2; Bey et al., 2001; Ikeda et al., 2017) were performed to assist in the interpretation of the sources and transport paths of observed BC in the Arctic Ocean. The horizontal resolution of GEOS-chem was 2° × 2.5° with 47 vertical layers from the surface to 0.01 hPa. The meteorological data was supplied by Modern-Era Retrospective analysis for Research and Applications, Version 2 (MERRA-2). Two BC tracers, namely anthropogenic BC (BCan) and biomass burning BC (BCbb), were defined for the simulations. The Evaluating of the Climate and Air Quality Impacts of Short-Lived Pollutants version 6b (ECLIPSEv6b) was adopted as anthropogenic emission source (Klimont et al., 2017). The Global Fire Emissions Database (GFED v4.1) with 0.25° × 0.25° of spatial resolution and daily temporal resolution was applied as biomass burning

https://doi.org/10.5194/egusphere-2023-2315
Preprint. Discussion started: 26 October 2023

emission source (van der Werf et al., 2017). In the following section, the simulated total BC mass concentration is noted as $m_{BC,S}$, and the simulated BC mass concentrations contributed by anthropogenic and biomass burning sources were noted as $m_{BC,SAN}$ and $m_{BC,SBB}$, respectively. Furthermore, the NOAA Air Resources Laboratory Hybrid Single-Particle Lagrangian Integrated Trajectory model (HYSPLIT; Stein et al., 2015) was also applied to assist the interpretation of BC sources.

4 Results and discussion

4.1 Spatial and temporal variations of BC mass concentrations

Figure 1 shows the shipborne observation cruise tracks North of 64° N during 2016–2020. Spatial distributions of the observed BC mass concentrations along the cruise tracks of respective years are indicated by filled color circles in Figs. 1b-f. For all the years, the cruises in the Arctic Ocean took place during August and early September, covering the region of 166° E –156° W and ≤80° N (Fig. 1a; Table 1). The cruise region in the Arctic in this study either fully or partially covered the shipborne research regions in previous studies by Taketani et al. (2016, 2022), Xie et al. (2007), Dall'Osto et al. (2020), Park et al. (2020), and Ding et al. (2018).

The temporal-spatial distribution of BC mass concentrations along the whole cruise tracks in respective years can be found in Fig. S1. To further investigate the spatial and temporal variations of observed BC, the m_{BC} in each cruise were categorized into three groups according to the latitude of the observations, i.e., South of 52° N (in the North Pacific Ocean), North of 72° N (mainly in the Canada Basin and the east part of the East Siberian Sea, which are noted as western central Arctic Ocean in the following sections of this study), and between 52 and 72° N (mainly in the Bering, Chukchi, and Beaufort Seas). They were statistically analyzed and the results are presented in Fig. 2. Time series of the m_{BC} and ship latitudes in each cruise are presented in Fig. 3. In general, m_{BC} in high latitude regions were relatively low and showed less temporal-spatial variations compared to low latitude regions. However, frequent high m_{BC} spikes were also observed at high latitudes in 2019. The high m_{BC} observed in lower latitude regions from the North Pacific Ocean to the southern Chukchi Sea near the Bering Strait can be explained by the fact that East Asia is the largest BC source region in the world (Ikeda et al., 2022) and that biomass burning in boreal regions including Siberia, Alaska, and Canada is also a large BC source in summer (Zhu et al., 2020).

Significant but not regular interannual variation of m_{BC} was observed in regions South of 52° N. The highest mean and median m_{BC} values were observed in 2018 and 2017, followed by 2019, 2020, and 2016 (Fig. 2a). At regions between 52 and 72° N and North of 72° N, except the year 2019, m_{BC} variations among other years were not evident (Fig. 2a). The median values of m_{BC} at the former region were 10–12 ng m^{-3} except for the cruise in 2019, when it was around 17 ng m^{-3}; at the latter region, the median values were 3–4 ng

https://doi.org/10.5194/egusphere-2023-2315
Preprint. Discussion started: 26 October 2023

m^{-3} except for 2019, when it was around 15 ng m^{-3}. The higher BC concentration and more frequent high BC spikes in 2019 than other years at the Arctic Ocean and marginal sea regions were likely affected by more frequent outflows of smoke from boreal vegetation fires during the cruise observation period (Sakerin et al., 2020). This is supported by a few pre-existing studies. For example, Antokhina et al. (2023) reported intensive fire activities during 3 July to 12 August 2019 in Eastern Siberia (95–120° E); Bhatt et al. (2021) reported extreme fire activity started in mid-August in Southcentral Alaska due to the extreme conditions of hot summer temperature and prolonged drought; Voronova et al. (2020) reported that the total burned-out areas and the amounts of emissions of fine aerosols in Siberia were abnormally high in 2019 especially in August; Chen et al. (2023) reported that unprecedented vegetation fires were observed in the eastern Siberia and Alaska in 2019; and Hayasaka (2022) reported that the number of hotspots in summer season in the Arctic region in 2019 was much greater than those in 2016–2018 and 2020. In addition, at Barrow observatory (Fig. 1a), the nearest surface station to the cruise regions in the Arctic Ocean of this study, the interannual variation of BC mass concentrations measured by a similar COSMOS instrument and absorption coefficient at 550 nm measured by two other filter-based absorption photometers in August and September also presented higher values in 2019 than in other years (Fig. S2; Ohata et al., 2021b; https://ads.nipr.ac.jp/dataset/A20201120-001; last access: 8 September 2022.), which is consistent with the interannual variations of BC mass concentrations observed in this study.

The BC mass concentration measured in the western central Arctic Ocean is comparable to those in previous studies. In this study, the median and mean (± 1 standard deviation) m_{BC} in August 2020 were 3.4 and 14 (±35) ng m^{-3}, respectively; the values are close to those measured in the central Arctic Ocean during the same period using a similar AE33 aethalometer, where the median and mean (± 1 standard deviation) values were 6.5 and 10 (±22) ng m^{-3}, respectively (Boyer et al., 2023). In addition, on 8–9 September 2016, when the *Araon* was cruising in the Arctic region similar to the observation region of Taketani et al. (2022) (i.e., approximately 70–74° N and 170–153° W), the mean (± 1 standard deviation) values of m_{BC} was 8.2 (±6.0) ng m^{-3}, which is consistent with that presented in Taketani et al. (2022, Fig. 2a) during the same period using a single particle soot photometer (SP2) (Moteki and Kondo, 2010). However, the overall mean m_{BC} observed in the Arctic Ocean of this study (10 ng m^{-3}, Table 1) is 10 times higher than that reported by Taketani et al. (2022). The large difference was likely caused by the spatial and temporal difference between the measurements in the two studies. The cruise routes in this study covered part of the East Siberian Sea region, whereas that in Taketani et al. (2022) was within the Chukchi and Beaufort Sea regions; and the cruise in this study occurred mainly in August whereas that in Taketani et al. (2022) mainly in September. Resultingly, different airmasses containing different BC concentrations could have been observed by this study and Taketani et al. (2022). Therefore, caution on the temporal and spatial ranges should be taken when comparing the mass concentrations of BC observed in the Arctic Ocean. This also indicates the

https://doi.org/10.5194/egusphere-2023-2315
Preprint. Discussion started: 26 October 2023

necessity to further study the spatial-temporal variations of BC in the Arctic Ocean. It is noted that the COSMOS can measure the BC mass concentration in the Arctic with ~10 % accuracy as compared with SP2 in 1 h time resolution (Ohata et al., 2019), therefore the instrument difference shouldn't have influenced the comparison between this study and Taketani et al. (2022) largely.

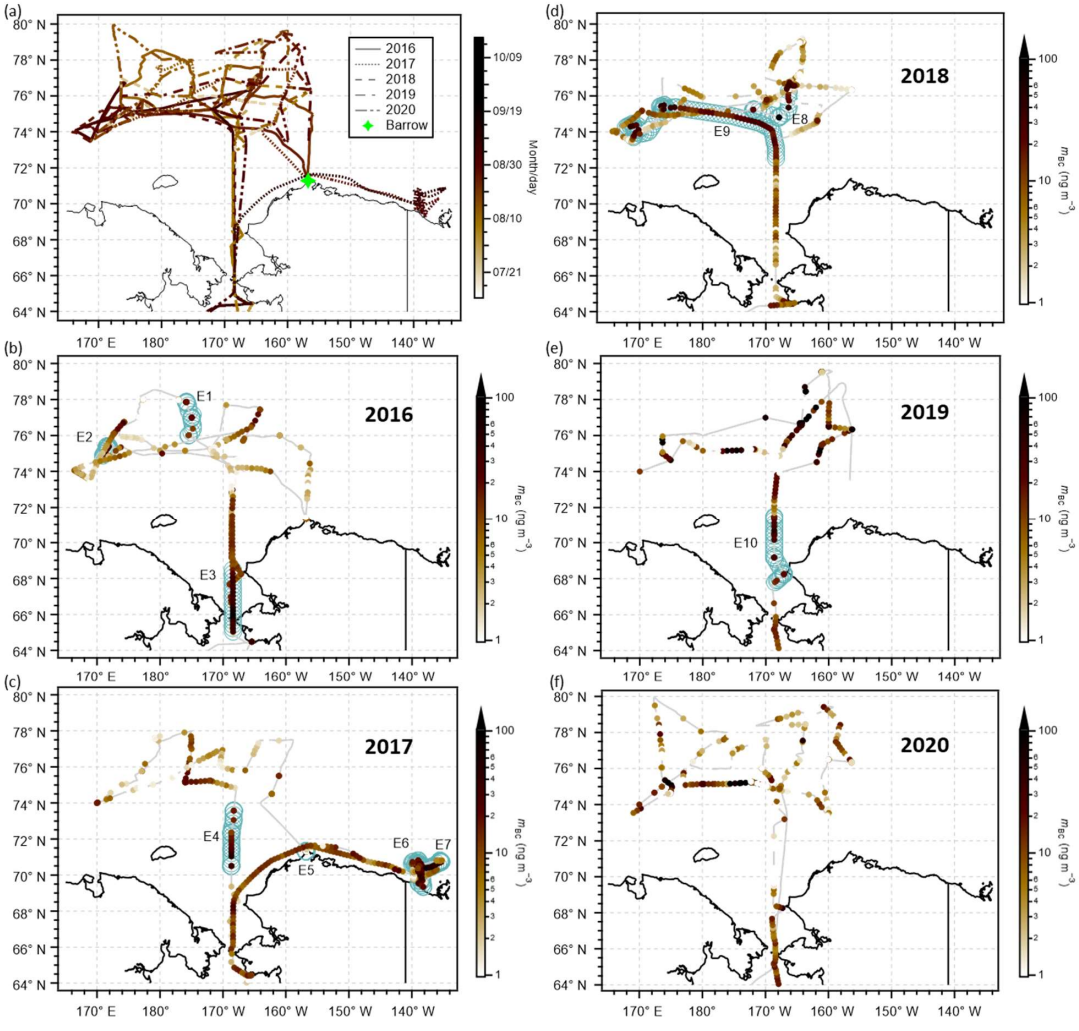

Figure 1 Shipborne observation cruise tracks North of 64° N during 2016–2020. (a) Color indicates month/day. Star marker indicates the location of the Barrow observatory (71.29° N, 156.75° W). (b-f) Spatial distribution of BC mass concentrations along the cruise tracks in respective years. The grey line represents the cruise track, and the filled color circle superimposed on the track indicates the BC mass concentration. The m_{BC} presented here is at 1 h time resolution and the data influenced by ship exhaust has

https://doi.org/10.5194/egusphere-2023-2315
Preprint. Discussion started: 26 October 2023

been removed. In panels (b-e), ship positions during the 10 episodes (E1-E10) were marked along the ship tracks as open circles. The temporal and spatial distribution of BC mass concentrations along the whole cruise tracks in respective years can be found in Fig. S1.

Table 1 Time and space coverage of R/V *Araon* and overall and background BC mass concentrations in the Arctic Ocean (≥72° N).

Year		**2016**	**2017**	**2018**	**2019**	**2020**
Period (month/day)		08/08–09/09	08/09–08/25	08/06–09/18	08/08–08/27	08/06–08/31
Latitude (°)		+72–+79	+72–+78	+72–+79	+72–+80	+72–+80
Longitude (°)		+166–−156	+170–−159	+166–−156	+170–−156	+169–−156
m_{BC}	**Overall**	10(±11)	6.6(±6.7)	7.8(±15)	73(±210)	14(±35)
(ng m^{-3})[a]	**Background**	3.1(±1.1)	3.6 (±2.2)	3.8 (±2.4)	-[b]	-[c]

[a] mean(± 1 standard deviation)
[b] No background period was identified.
[c] Criteria for background periods were not applicable because the data was obtained from an aethalometer.

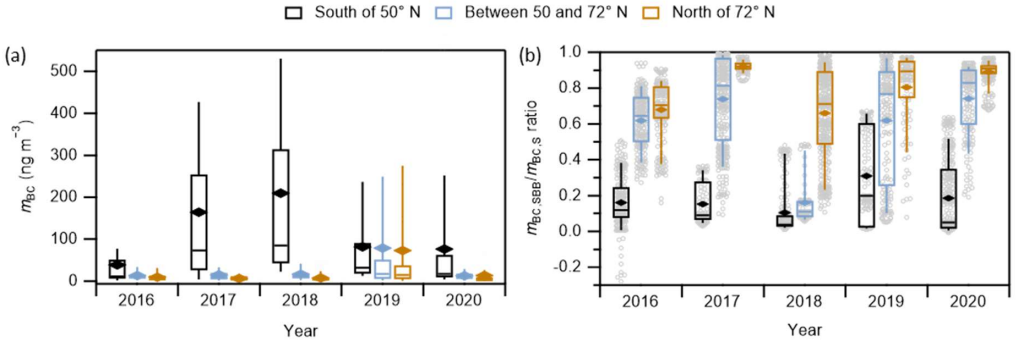

Figure 2 Box plots of (a) the observed BC mass concentration and (b) the model simulated ratio of biomass burning BC to total BC ($m_{BC,SBB}/m_{BC,S}$) along the ship tracks at latitudes south of 52° N, north of 72° N, and between 52 and 72° N for respective cruises in 2016–2020. Lower whisker – 9th percentile; upper whisker – 91st percentile; box bottom – first quartile; box top – third quartile; line in the box – median value; solid diamond marker – arithmetic mean. In panel (b), individual data are presented as grey open circles.

https://doi.org/10.5194/egusphere-2023-2315
Preprint. Discussion started: 26 October 2023

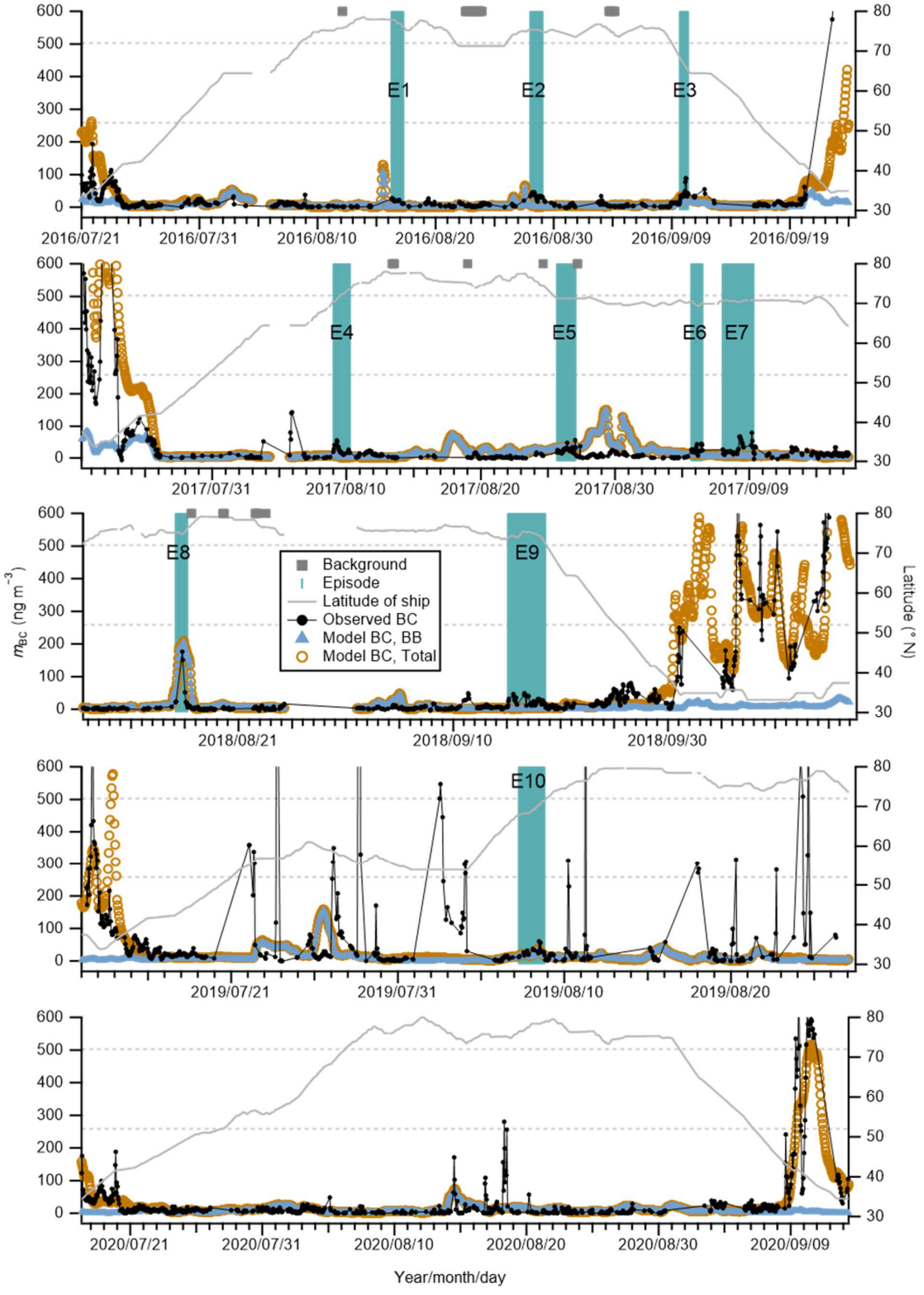

https://doi.org/10.5194/egusphere-2023-2315
Preprint. Discussion started: 26 October 2023

Figure 3 Time series of mass concentrations of observed BC, model simulated total BC and biomass burning BC, and latitude of ship positions. The Arctic Ocean background periods defined in Sect. 4.2 and 10 high BC episodes (E1 to E10) are also shown. The short dashed light gray lines represent latitudes 52° N and 72° N. The time series of raw 1-h m_{BC} before removing the influence of ship exhausts are presented in Fig. S3.

4.2 Background BC concentration in the western central Arctic Ocean

To evaluate the air quality and climate changes in the Arctic correctly, it is important to estimate the background BC mass concentration in the Arctic. Ideally, the Arctic Ocean is one of the pristine regions in the world and background concentrations of primary air pollutants such as black carbon there should be close to zero. However, zero background black carbon may not be true to the Arctic marine boundary layer atmosphere due to the influence of many anthropogenic and natural activities that bring BC aerosols to the Arctic Ocean. Those activities include anthropogenic productive activities producing large amount of air pollutants in low latitude regions that may export to the Arctic through long-range transport (Ikeda et al., 2017; Zhu et al., 2020), gas flaring and wildfire frequently occurring in the Arctic regions (Stohl et al., 2013), as well as expanding local activities such as commercial fisheries and cruise tourism along the Arctic coastal region along the Arctic climate warming (AMAP, 2021b). In winter and early spring, the buildup of anthropogenic pollutions, due to the expansion of the polar dome, which allows transport of anthropogenic pollutants from continental regions further south, and the stable atmospheric conditions, can lead to monthly mean m_{BC} of as high as more than 100 ng m^{-3} (e.g., Boyer et al., 2023). In summer and early autumn, while intense wildfires in the boreal regions can result in remarkably high m_{BC} levels, as discussed in Sect. 4.1, the m_{BC} in the Arctic Ocean surface atmosphere can be extremely low due to changes in transport patterns and wet deposition processes that efficiently remove transported anthropogenic aerosols (e.g., Sierau et al., 2014). Therefore, summer and early autumn months are the most suitable months to evaluate the background level of m_{BC} in the Arctic Ocean.

The background periods in the western central Arctic Ocean (>72° N) were defined according to the m_{BC} measured by COSMOS and the 5 day HYSPLIT back trajectories as follows: the 1-min m_{BC} was below the lowest detection limit of 50 ng m^{-3} for continually 2 hours or longer, the 1-h m_{BC} was above the lowest detection limit of 1 ng m^{-3}, and the air masses were from the Arctic Ocean. As shown in Fig. 3, background periods were identified for the cruises in 2016, 2017, and 2018. The overall mean of background m_{BC} calculated from m_{BC} at 1 h time resolution for 53 hours was 3.3 (±1.5) ng m^{-3} (Table 1). This value is lower than the mean BC mass concentrations in regions North of 72° N (Table 1), which indicates that the Arctic Ocean could be frequently affected by local or regional BC pollutants. In addition, this value is lower than the overall mean BC mass concentration of 10 (±22) ng m^{-3} in the central Arctic Ocean in August 2020

https://doi.org/10.5194/egusphere-2023-2315
Preprint. Discussion started: 26 October 2023

measured by an aethalometer (Boyer et al., 2023), which suggests that even in the summer months the central Arctic Ocean could be affected by imported BC pollutants (Boyer et al., 2023; Sierau et al., 2014). Note that the estimated BC mass concentration in Boyer et al. (2023) might be twice the actual values because the default parameter settings of AE33 were used (Sect. 2).

To our knowledge, this is the first study that calculated the background concentration of BC in the Arctic marine boundary layer during summer periods. The result should be representative as the data covered the summer seasons of three years. Nevertheless, the data are mostly limited to within the western Arctic Ocean, and the minimum limit of 1 ng m^{-3} for 1-h m_{BC} in the definition of background conditions may have elevated the overall estimation of background m_{BC}. Therefore, more studies over broader areas in the Arctic Ocean using instruments with lower detection limits such as SP2 (e.g., Taketani et al., 2022) are warranted to make a conclusion on the background BC concentration of contemporary Arctic atmosphere.

4.3 Comparisons between observations and model simulations

The time series of GEOS-Chem model simulated total BC mass concentration ($m_{BC,S}$) and that were ascribed to biomass burning sources ($m_{BC,SBB}$) are also presented in Fig. 3, which shows that GEOS-Chem overestimated some low m_{BC} (e.g., during 28 August – 5 September 2017) and underestimated some high m_{BC} (e.g., 18 August 2020). Scatter plots between $m_{BC,S}$ and m_{BC} are presented in Fig. S4. Except for the 2019 cruise, the Pearson correlation coefficient (R) values in other years were greater than 0.5. The R for the overall model versus observed m_{BC} is 0.66. Therefore, GEOS-Chem model can reproduce (0.66 × 0.66 =) 44 % of the temporal and spatial variations of the shipborne m_{BC}. The normalized mean biases of model simulated from observed m_{BC} in 2017 and 2019 were high and were 102.9 % and −37.4 %, respectively. The overall normalized mean bias was estimated to be 4.6 %. In addition, Fig. S4 shows systematical overestimation of model m_{BC} in the region of lower than 1 ng m^{-3}. Similar overestimation was also found in Whaley et al. (2022), which was possibly caused by the coarse resolution of the GEOS-Chem model, making it unable to accurately simulate such low BC mass concentrations.

GEOS-Chem failed to reproduce almost all the high BC spikes observed in the Arctic Ocean in 2019. As discussed in Sect. 4.1, the high spikes in 2019 were likely caused by intensive wildfires in the Arctic especially Eastern Siberia (Antokhina et al., 2023) and Alaska (Bhatt et al., 2021). Therefore, we can infer that the less accounting of wildfires in the boreal regions by the GFED4 biomass burning inventory used in this study might be the main reason for the poor reproduction of observed BC during the 2019 cruise by GEOS-Chem (Pan et al., 2020) considering that the transport path of BC from the boreal regions to the Arctic Ocean is mainly through the lower to middle atmosphere as indicated by the analyses in Sect. 4.4 and previous studies (e.g., Ikeda et al., 2017; AMAP, 2021a). Thus, it is necessary to improve the estimation of biomass burning emissions in the boreal regions. However, the influence of possible uncertainties in the

https://doi.org/10.5194/egusphere-2023-2315
Preprint. Discussion started: 26 October 2023

transport regime of the GEOS-Chem model (e.g., overestimation of wet deposition) in reproducing the peaks observed during the 2019 Arctic cruise cannot be ruled out.

4.4 Sources of High BC episodes

Statistical analyses of the GEOS-Chem simulated biomass burning BC to total BC ratio ($m_{BC,SBB}/m_{BC,S}$) are presented in Fig. 2b, which indicate that BCbb accounted for more of the observed BC mass concentration in higher than in lower latitude regions. In the Arctic Ocean (i.e., north of 72° N), BCbb contributed on average 67–92 % of total BC observed along the cruise tracks. In the marginal Arctic Sea regions (i.e., between 52 and 72° N), $m_{BC,SBB}/m_{BC,S}$ was estimated to be 62–74 % except in the 2018 cruise, where it was estimated to be 16 % (Fig. 2b). These results indicate that most of the observed BC in the Arctic during summer and Autumn were from biomass burning sources.

Elevated BC mass concentration periods were observed in almost every Arctic cruises (Fig. 3). To characterize the sources of the high concentrations of BC in the Arctic Ocean and the marginal seas, high BC episodes were defined as periods when the 1-h m_{BC} was continually greater than 10 ng m^{-3} for 18 h or longer and the mean of valid 1-h m_{BC} during the defined periods was greater than 20 ng m^{-3}. In total, 10 high BC mass concentration episodes were identified (Figs. 1, 3, S1, and S3, Table 2). Episode 1 (abbreviated as E1, same for other episodes) and E8 were observed in the Arctic Ocean; E2 was observed in the East Siberian Sea; E3 was observed on the way from the Chukchi Sea to the Bering Strait; E4 and E10 were observed in the Chukchi Sea; E5, E6, and E7 were observed in the Beaufort Sea near the Alaska coast; and E9 was observed on the way from the East Siberian Sea to the Chukchi Sea. Table 2 presents the time and space range details and observed and model simulated mean BC mass concentrations during the 10 episodes. Note that in addition to these 10 episodes, high BC was also observed in the Arctic at other times, such as on 14–18 August 2020.

According to GEOS-Chem model simulation results, except for E9 which occurred in 2018, biomass burning contributed more than 69 % of the observed BC during all the other episodes (Table 2). Furthermore, the temporal and spatial variations of E3, E8, and E10 were well reproduced by GEOS-Chem model (Fig. 3). Therefore, in the following, the sources of BC during E3, E8, and E10 are elaborated based on GEOS-Chem model as well as HYSPLIT back trajectory model.

Table 2 Time and space ranges and observed and simulated BC mass concentrations for the 10 episodes.

Episodes	Start time	Duration (h)		Latitude (°)	Longitude (°)	Mean m_{BC} (ng m^{-3})		$m_{BC,SBB}/m_{BC,S}$[c] (%)
		Total[a]	Valid[b]			Observed	Model, total	
E1	16 Aug 2016, 06:00	25	14	+76.00–+77.88	−175.89–−174.78	19.7	0.991	82

https://doi.org/10.5194/egusphere-2023-2315
Preprint. Discussion started: 26 October 2023

E2	28 Aug 2016, 00:00	26	25	+74.89–+75.40	+170.93–+171.86	34.4	2.94	72
E3	9 Sep 2016, 16:00	18	18	+65.05–+68.48	−168.48–−168.41	44.1	25.4	69
E4	9 Aug 2017, 00:00	31	19	+70.49–+73.58	−168.71–−168.28	25.1	5.56	82
E5	25 Aug 2017, 16:00	34	32	+71.32–+71.33	−156.88–−156.79	25.3	32.8	97
E6	4 Sep 2017, 16:00	21	17	+69.34–+70.57	−139.02–−138.21	26.0	11.4	73
E7	7 Sep 2017, 00:00	56	30	+70.38–+70.81	−140.02–−135.31	31.5	7.31	87
E8	15 Aug 2018, 03:00	27	9	+74.80–+76.26	−171.97–−166.32	55.4	154	98
E9	15 Sep 2018, 02:00	84	50	+72.52–+75.50	+167.84–−168.36	24.7	3.54	41
E10	7 Aug 2019, 06:00	38	21	+67.80–+71.50	−168.67–−167.12	28.9	23.4	86

[a] The total duration of each episode.
[b] The number of hours with valid 1-h BC mass concentration data in each episode.
[c] GEOS-Chem simulated biomass burning to total BC mass concentration ratio.

4.4.1 Episode 3

Episode 3 occurred during 9 September 2016, 16:00 – 10 September 2016, 10:00 UTC. The mean m_{BC} is 44 ng m^{-3} and BC from biomass burning was estimated to contribute 69 % of the total BC (Table 2). Figure 4 presents the surface distribution of BCbb and the surface winds before this episode. It suggests that the biomass burning occurred on boarder of Chukotka Autonomous Okrug (CAO) and Kamchatka Krai (KamK) was likely the main source of this episode. Southwest winds have brought the biomass burning BC containing airmass from the source region to the ship positions. Contour plots in Fig. 4 indicate that biomass burning contributed 80 % of the BC mass concentration at this source region. GFED4 data and back trajectories (Fig. S5) also indicate that biomass burning occurred on boarder of CAO and KamK was likely the main source of the observed high BC mass concentration during E3. The longitude-height cross sections of BCbb also presented in Fig. 4 suggests that the height of the transport path of BCbb was constrained to >700 hPa (i.e., <~3 km) and little contribution of subsidence BC from upper atmosphere had contributed to E3. This is also supported by the height distributions of back trajectories (Fig. S5), which indicate that the observed airmasses were transported to the ship position within 2.5 km above the ground level. Compared with BCbb, the contribution of anthropogenic BC to the observed high BC mass concentrations in E3 was relatively small through either surface level or above-ground transports (Fig. S6).

https://doi.org/10.5194/egusphere-2023-2315
Preprint. Discussion started: 26 October 2023

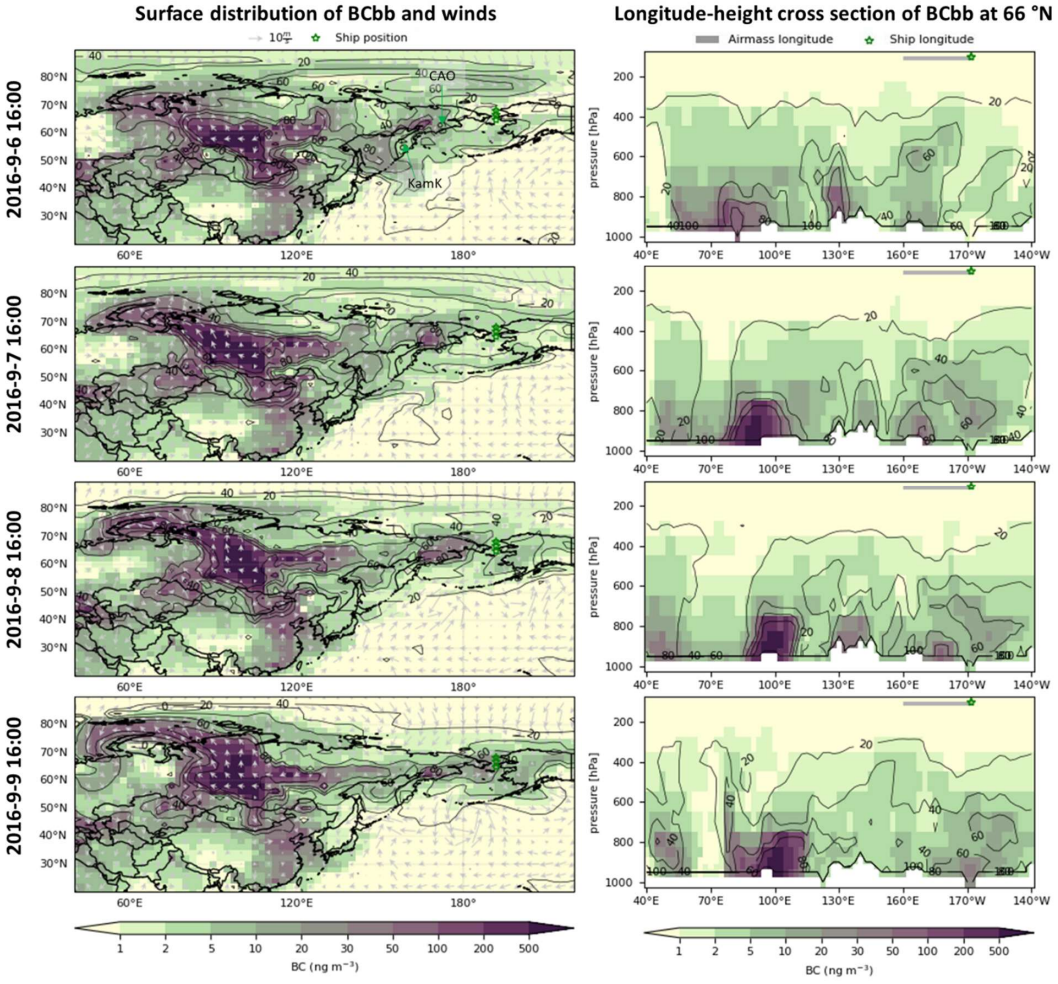

Figure 4 Simulated biomass burning BC (BCbb, color image) surface distributions (left) and longitude-pressure cross sections at 66° N (right) before Episode 3. Superimposed on the left panels are surface winds and the ship positions. Superimposed on the right panels are the ship longitude positions and the possible transport region of BC-containing air masses related with Episode 3. The latter was inferred from GEOSChem model (left) and back trajectories (Fig. S5). On both panels, the contour plot represents the simulated biomass burning BC to total BC ratio (%). In the upper left panel, CAO-Chukotka Autonomous Okrug and KamK-Kamchatka Krai.

4.4.2 Episode 8

Episode 8 occurred during 15 August 2018, 3:00 – 16 August 2018, 6:00 (Fig. 3). The mean m_{BC} is 55 ng m^{-3} and BC from biomass burning was estimated to contribute 98 % of the total BC (Table 2). Note that although there are only nine valid 1-h m_{BC} during E8, following analyses on gaseous species and GEOS-

https://doi.org/10.5194/egusphere-2023-2315
Preprint. Discussion started: 26 October 2023

Chem and back trajectory model simulations indicate that E8 is part of a prominent transport event of Siberia biomass burning airmasses to the Arctic Ocean. Figure 5 presents the surface distribution of biomass burning BC and surface winds before to after Episode 8. Biomass burning airmasses from Krasnoyarsk Krai (KraK) and the Republic of Sakha (Sakha) were transported northwards and northeastwards to the Siberia Arctic and then spread eastwards by the westerly from 13 to 14 August. Further, northwest winds blew the biomass burning BC containing airmasses to the ship positions on 15 August. Contour plots in Fig. 5 indicate that biomass burning contributed more than 80 % of BC mass concentration in the transported airmasses. These transport paths are also supported by GFED4 data and back trajectory analyses (Fig. S7). Figure 5 also shows that the biomass burning BC containing airmass was blown away from the ship later by northerly winds. Although the height distribution of back trajectories presented in Fig. S7 showed that the observed air masses during E8 were transported to the ship position mainly under 2 km above the ground, longitude-height distributions of BCbb presented in Fig. 5 indicate that the transport of biomass burning BC containing airmasses from the source regions to above the ship position was mainly through lower to middle atmosphere. Although the contribution of anthropogenic BC to the observed BC in Episode 8 was very small, surface level concentration distribution and longitude-height cross sections (Fig. S8) show that they followed similar transport paths to the ship positions as the biomass burning BC.

Figure 6 presents the time series of the atmospheric mixing ratios of CO, CH_4, CO_2, and O_3, as well as observed and model simulated BC mass concentrations during the 2018 shipborne observation when CO, CH_4, and CO_2 data were obtained. During Episode 8, the mixing ratios of CO and CH_4 increased whereas those of CO_2 and O_3 were not or even slightly decreased. Similar phenomena have been reported in previous studies in the lower atmosphere over Siberia (Paris et al., 2010). The increased CO and CH_4 is consistent with the observation of biomass burning plumes possibly related with smoldering combustion conditions (Andreae et al., 1994). The decrease in CO_2 is possibly due to uptake by intact high latitude vegetation during the polar daylight period before transporting to the Arctic Ocean (Paris et al., 2010) as well as smoldering combustion conditions, producing much more CO than CO_2. The former is consistent with the fact that in Siberia planetary boundary layer and free troposphere CO_2 concentrations are at the minimum in July to August (Sasakawa et al., 2013). The no increase or slight decrease of O_3 was possibly caused by less active photochemistry in the fire plumes, in particular, at the northern high-latitude (Tanimoto et al., 2000) and/or surface deposition (Text S1). Over Siberia, the O_3 formed in biomass burning plumes probably was lost greatly due to deposition to the forest canopy before being transported out of the Siberia terrestrial to the Arctic Ocean (Chin et al., 1994; Paris et al., 2010) so that the observed O_3 concentration in the plumes were lower than that of the Arctic Ocean background. Scatter plots between m_{BC} versus CO, O_3 versus CO, CO versus CO_2, and CH_4 versus CO_2 are presented in Fig. 7, where most of the data points during E8 are significantly different from the others. The reduced major axis regression between O_3 and CO during period

https://doi.org/10.5194/egusphere-2023-2315
Preprint. Discussion started: 26 October 2023

having not been influenced by Episode 8 airmasses resulted in a slope of 0.39, which is similar to that derived from the MOSAiC observation in the central Arctic during the same season of 2020 (Fig. S9; Angot et al., 2022 and references therein). The spatial distribution of the atmospheric mixing ratios of O_3, CO, CO_2, and CH_4, and the $m_{BC}/\Delta CO$ (i.e., the enhancement ratio of BC to CO; here, ΔCO is the increase in CO relative to baseline, see the caption of Fig. 8 for more details; note that in order to obtain more $m_{BC}/\Delta CO$ data points, the background of m_{BC} was not subtracted) and CO/CO_2 ratios are presented in Fig. 8. Distinctive features such as increases of CO, CH_4, $m_{BC}/\Delta CO$ and CO/CO_2 ratios and decreases of CO_2 and O_3 during E8 can be clearly observed. In addition, the median $m_{BC}/\Delta CO$ of less than 1 ng m^{-3} ppb^{-1} is near to those reported in Taketani et al. (2022), which might have been affected by wet removal of BC during transport processes or smoldering combustion conditions.

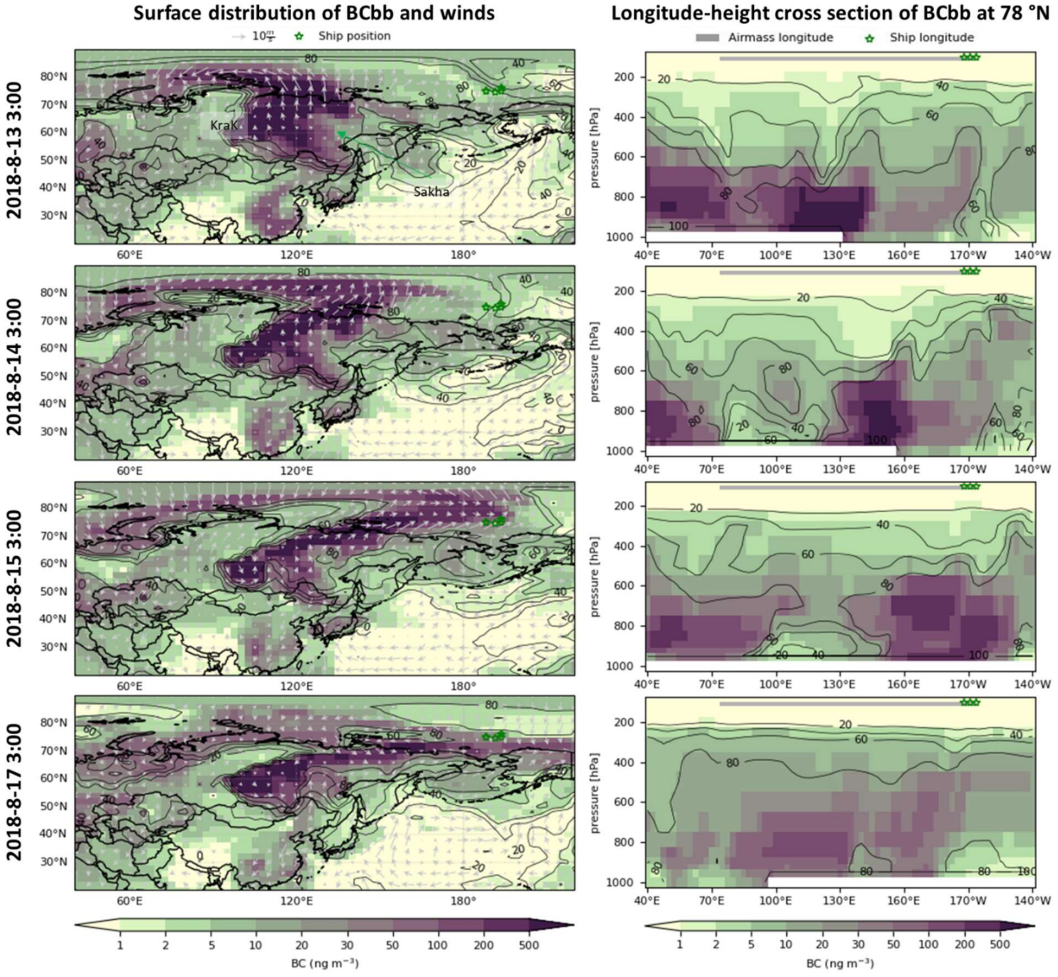

https://doi.org/10.5194/egusphere-2023-2315
Preprint. Discussion started: 26 October 2023

Figure 5 Simulated biomass burning BC (BCbb, color image) surface distributions (left) and longitude-pressure cross sections at 78° N (right) before to right after Episode 8. Superimposed on the left panels are surface winds and the ship positions. Superimposed on the right panels are the ship longitude positions and the possible transport region of BC-containing air masses related with Episode 8. The latter was inferred from GEOSChem model (left) and back trajectories (Fig. S7). On both panels, the contour plot represents the simulated biomass burning BC to total BC ratio (%). In the upper left panel, KraK- Krasnoyarsk Krai and Sakha- the Republic of Sakha.

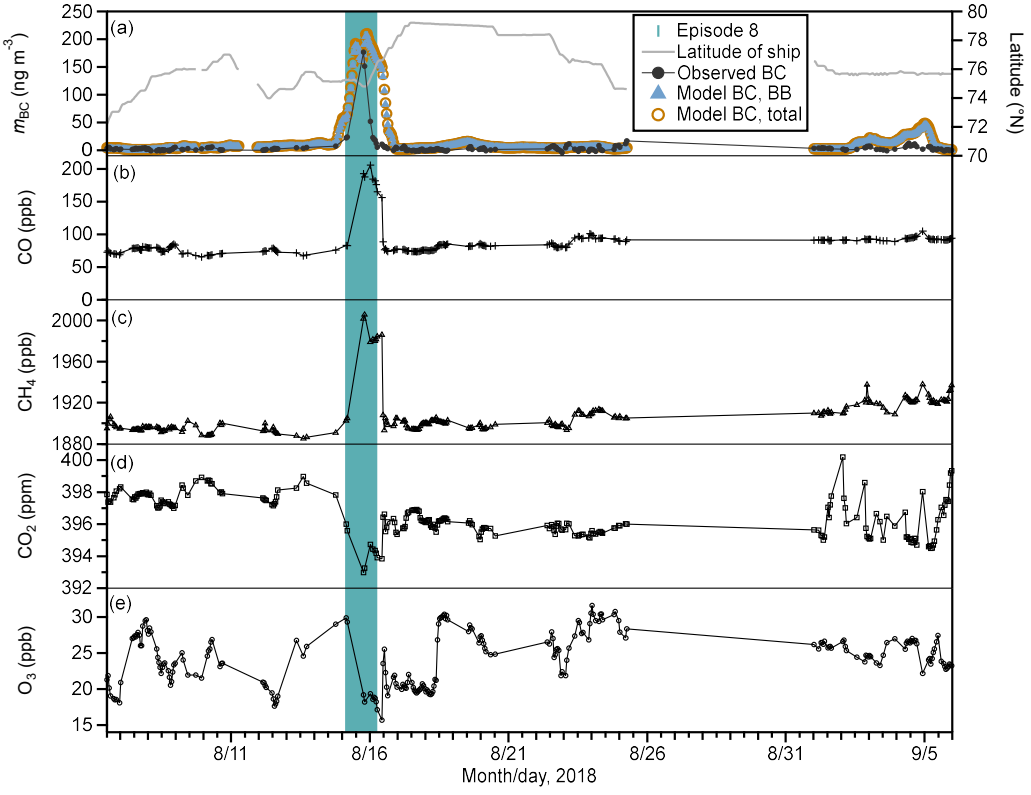

Figure 6 Time series of (a) observed BC, model simulated total BC and biomass burning BC, and latitude of ship positions, (b) CO, (c) CH_4, (d) CO_2, and (e) O_3 during the 2018 shipborne observation. Bar shade indicates the Episode 8 period.

https://doi.org/10.5194/egusphere-2023-2315
Preprint. Discussion started: 26 October 2023

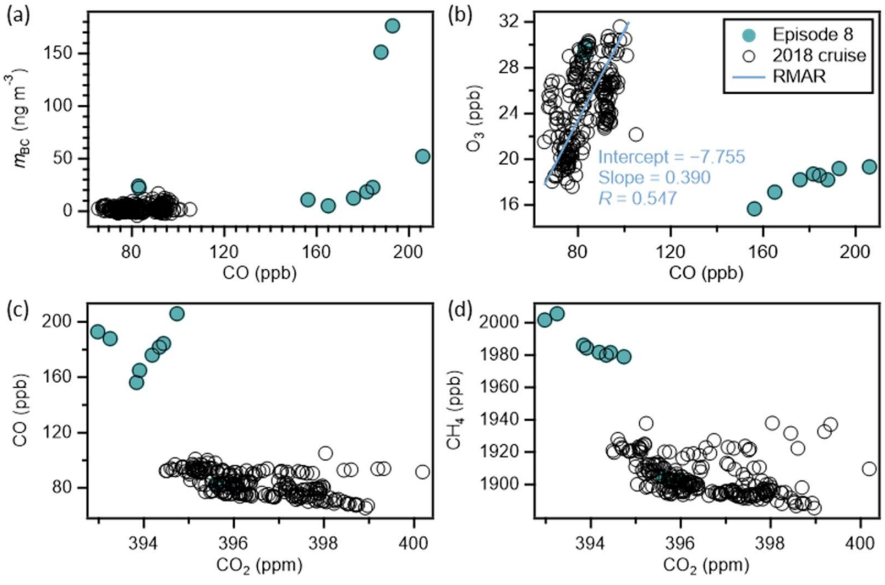

Figure 7 Scatter plots of (a) m_{BC} versus CO, (b) O_3 versus CO, (c) CO versus CO_2, and (d) CH_4 versus CO_2 during the cruise in the Arctic Ocean in 2018 and Episode 8. In panel (b), the line represents the reduced major axis regression (RMAR) for data having not been influenced by Episode 8 airmasses: the intercept, slope, and correlation coefficient are also presented.

https://doi.org/10.5194/egusphere-2023-2315
Preprint. Discussion started: 26 October 2023

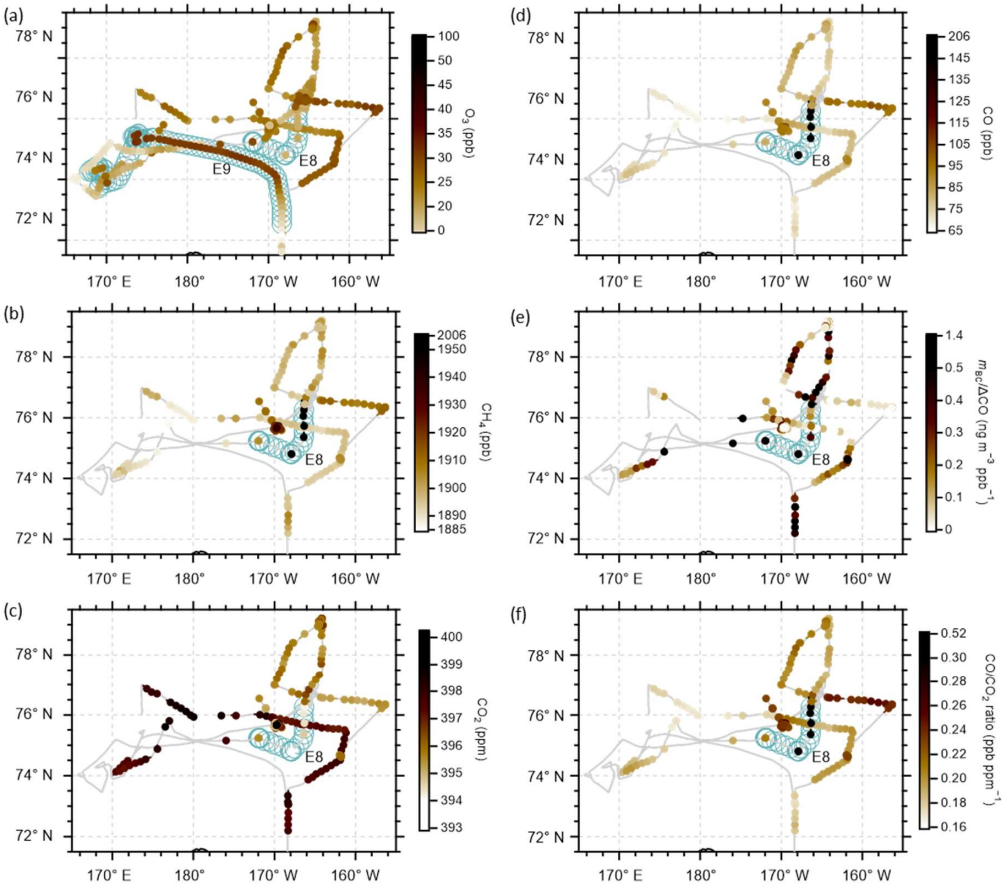

Figure 8 Surface distributions of O_3 (a), CO (b), CO_2 (c), and CH_4 (d) mixing ratios, and $m_{BC}/\Delta CO$ (e) and CO/CO_2 (f) ratios along the ship track during part of the 2018 cruise in the Arctic Ocean. In each panel, the grey line represents the cruise track; the filled color markers superimposed on the track indicates the respective observed (a, b, c, and d) or derived (e and f) parameters, which are at 1 h time resolution and screened to remove the influence of ship exhausts; and the open circles represent the ship positions during Episodes 8 (a-f) and 9 (a). Note that valid CH_4, CO, and CO_2 data are only available for a limited time (Fig. 6). For the derivation of ΔCO, the baseline of CO is defined as the minimum 1-h CO data; and $m_{BC}/\Delta CO$ ratio was calculated only when ΔCO was higher than 4 ppb.

4.4.3 Episode 10

Episode 10 occurred during 7 August 2019, 6:00 – 8 August 2019, 20:00 UTC (Fig. 3). The mean m_{BC} is 29 ng m^{-3} and BC from biomass burning was estimated to contribute 86 % of the total BC (Table 2). Figure 9 presents the surface distribution of biomass burning BC and surface winds before and during Episode 10. Although no obvious fire spot was observed on boarders among Magadan Oblast and Chukotka

https://doi.org/10.5194/egusphere-2023-2315
Preprint. Discussion started: 26 October 2023

Autonomous Okrug and Kamchatka Krai (abbreviated as MCK boarders, Figs. 9 and S10), GEOS-Chem simulations showed high concentration of biomass burning BC at MCK boarders on 6 August 2019 (Fig. 9), which was then transported to the ship position by weak northeastward winds. Longitude-pressure cross sections of BCbb presented in the right panels of Fig. 9 suggest that the high BCbb occurred at MCK boarders (150–170° E) was likely subsidence from upper atmosphere. Surface BCbb distributions (Fig. 9) and GFED4 map (Fig. S10) show that intensive biomass burning occurred in Krasnoyarsk Krai (KraK), Irkutsk Oblast (IrO), and the Republic of Sakha (Sakha) areas (90–150° E) before and during Episode 10. This is consistent with Antokhina et al. (2023), which reported intensive fire activities during 3 July to 12 August 2019 in Siberia (95–120° E). The highly BCbb containing airmasses from these intensive fires advected up to 4 km (i.e., ~600 hPa) and transported to the ship position mainly through the lower to middle atmospheres (Fig. 9right). Figures S11 and S12 show the horizontal BCbb distribution and wind fields at about 800 and 600 hPa, respectively. Both figures indicate that subsidence of BCbb containing airmasses occurred at MCK boarders, and the rest of BCbb containing airmasses were transported to the Arctic above the ship positions through much stronger than surface southwest winds, which are consistent with the longitude-pressure cross section of BCbb (Fig. 9). In addition, the height distribution of back trajectories also showed that more than a third airmasses originated from an altitude higher than 2 km (Fig. S9). Contour plots superimposed on each figure (Figs. 9 and S11-12) indicate that biomass burning BC contributed to more than 80 % of the BC transported to the ship position. Surface distributions and longitude-height distributions (Fig. S13) of anthropogenic BC show that it contributed little to the observed BC in Episode 10.

https://doi.org/10.5194/egusphere-2023-2315
Preprint. Discussion started: 26 October 2023

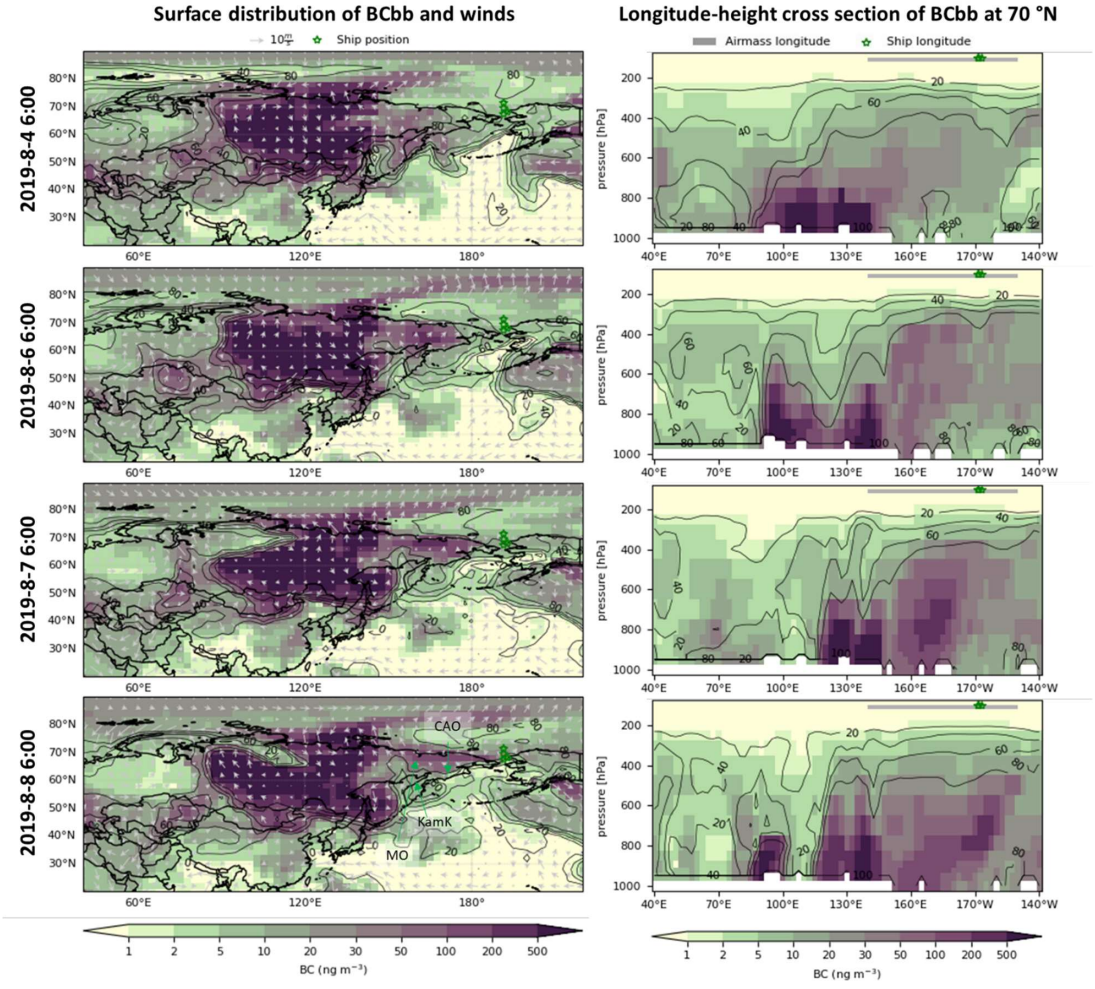

Figure 9 Simulated biomass burning BC (BCbb, color image) surface distributions (left panel) and longitude-pressure cross sections at 70° N (right panel) before and during Episode 10. Superimposed on the left panels are surface winds and the ship positions. Superimposed on the right panels are the ship longitude positions and the possible surface transport region of BC-containing air masses related with Episode 10. The latter was inferred from GEOSChem model (left) and back trajectories (Fig. S10). On both panels, contour plots represent the simulated biomass burning BC to total BC ratio (%). In the lower left panel, MO- Magadan Oblast, CAO- Chukotka Autonomous Okrug, and KamK- Kamchatka Krai.

5 Summary and conclusions

The mass concentration of black carbon aerosols was measured in the Arctic Ocean, encompassing the western Arctic Ocean and part of the East Siberian Sea, along with the North Pacific Ocean using light

https://doi.org/10.5194/egusphere-2023-2315
Preprint. Discussion started: 26 October 2023

absorption methods on board icebreaker R/V *Araon* during summer and autumn 2016–2020. Relatively low m_{BC} were observed at higher than low latitude regions. In the Arctic Ocean (>72° N), the overall mean (± 1 standard deviation) of 1-h m_{BC} during the cruises in 2016, 2017, 2018, 2019, and 2020 were 10 (±11), 6.6 (±6.7), 7.8 (±15), 73 (±210), and 14 (±35) ng m^{-3}, respectively; the background m_{BC} concentration was estimated to be 3.3 (±1.5) ng m^{-3}. In the Arctic Ocean and the Bering Sea (>52° N), the year-to-year variation of m_{BC} was not significant, except for the 2019 cruise, which observed much higher and more frequent elevated m_{BC} compared to other years. This increase was likely attributed to more frequent biomass burning in the Arctic region in 2019. We identified 10 high BC episodes in the observational data based on specific criteria: 1-h m_{BC} greater than 10 ng m^{-3} for a continuous duration of more than 18 h, with an overall mean of valid m_{BC} during the episodes exceeding 20 ng m^{-3}.

Tagged tracer simulations of BC using a global chemistry transport model (GEOS-Chem) were applied for the interpretation of the sources and transport paths of the observed BC. GEOS-Chem analyses indicate that biomass burning composed the largest contribution to the observed BC along the ship tracks in the Arctic Ocean (67–92 %) and the elevated BC mass concentration episodes (41–98 %). GEOS-Chem also revealed that transport paths of biomass burning BC from Siberian area to the Arctic could occur near-surface and/or through the lower to middle atmosphere. However, GEOS-Chem failed to accurately replicate the frequently observed high BC spikes in the Arctic during the 2019 cruise, which were attributed to the influx of biomass burning airmasses. This suggests the need for improvements in biomass burning emission inventories, especially considering the ongoing increase in wildfires during the boreal summer in a warming climate. Nevertheless, it cannot be ruled out that uncertainties in the BC transport regimes used in GEOS-Chem also contributed to the simulation discrepancies.

This study provides crucial datasets on BC mass concentrations and the mixing ratios of O_3, CH_4, CO, and CO_2 in the western Arctic Ocean regions during summer and autumn. Our results also highlight the significant impact of boreal fires on the observed Arctic BC during summer and early autumn months, consistent with previous modelling and observational studies (e.g., Zhu et al., 2020; Popovicheva et al., 2022). These results are valuable for model validation, predicting Arctic climate change, and guiding air quality research in the Arctic Ocean. In addition, due to rapid changes in temperature, precipitation, snow cover, sea and land ice, permafrost, and extreme events occurring in the Arctic (AMAP, 2021b), the sources, transport pathways, and climate forcing effects of BC are thought to be changing in the Arctic. Therefore, further studies on the spatial-temporal distributions, background concentrations of BC in the Arctic marine boundary layer, and the impact of boreal fires as well as other natural and anthropogenic sources on Arctic Ocean atmospheric BC are required to clearly understand the feedback of atmospheric BC in the rapidly changing Arctic Ocean.

https://doi.org/10.5194/egusphere-2023-2315
Preprint. Discussion started: 26 October 2023

Appendix A: Statistics of gaseous species

Table A1: Statistics of the observed concentrations of gaseous species during shipborne measurements in 2017 and 2018.

Year		2017	2018					
Species		O_3 (ppb)	O_3 (ppb)	CH_4 (ppb)	CO (ppb)	CO_2 (ppm)	CO/CO_2 ratio (ppb ppm^{-1})	m_{BC}/ΔCO ratio (ng m^{-3} ppb^{-1})
North of 72° N	Median	23.2	24.2	1900.7	82.2	396.21	0.208	0.119
	Mean	24.3	23.6	1906.8	86.4	396.46	0.218	0.172
	STD	3.6	5.0	19.1	20.3	1.23	0.052	0.238
Between 52 and 72° N	Median	25.8	24.8	-	-	-	-	-
	Mean	25.1	24.1	-	-	-	-	-
	STD	6.1	6.0	-	-	-	-	-
South of 52° N	Median	38.9	38.8	-	-	-	-	-
	Mean	38.0	43.2	-	-	-	-	-
	STD	12.9	14.3	-	-	-	-	-
Whole cruise	Median	25.1	26.8	-	-	-	-	-
	Mean	27.2	29.3	-	-	-	-	-
	STD	8.9	12.5	-	-	-	-	-

Note: STD, standard deviation; -, no available data.

Data availability

The dataset containing m_{BC} (ng m^{-3}), ship latitude and longitude, relative wind direction (RWD), relative wind speed (RWS, m s^{-1}), CH4 (ppb), CO (ppb), and CO2 (ppm) used in this publication is available online (Deng et al., 2023; https://db.cger.nies.go.jp/MD/10.17595/202307XX.001.html.en; last access: 25 September 2023).

Author contributions

HT, SK, and JJ designed the experiment and did the shipborne observations with contributions from SO, YJY, EJY, and SHK; KI did the model simulations; YD analyzed the observation and model data with contributions from HT and KI; YD made the manuscript with contributions from HT and KI; and all authors contributed to the revisions of the manuscript.

Competing interests

The authors declare no competing interests.

Acknowledgements

We thank Ms. Kimiko Suto for her support in gaseous species data analysis. We acknowledge the NOAA Air Resources Laboratory (ARL) for providing the HYSPLIT transport and dispersion model. This research

https://doi.org/10.5194/egusphere-2023-2315
Preprint. Discussion started: 26 October 2023

was supported by the Korea Institute of Marine Science & Technology (KIMST) funded by the Ministry of Oceans and Fisheries, Korea (grant no. 20210605, Korea-Arctic Ocean Warming and Response of Ecosystem, KOPRI). Financial support to NIES was given by the Environmental Research and Technology Development Fund (ERTDF) from the Ministry of the Environment, Japan (grant no. 2-2201: JPMEERF20222001), and by JSPS KAKENHI grant number JP21K12216 and JP17KK0016.

References

AMAP: AMAP Assessment 2015: Black carbon and ozone as Arctic climate forcers, Oslo, Norway, 2015.

AMAP: AMAP Assessment 2021: Impacts of Short-lived Climate Forcers on Arctic Climate, Air Quality, and Human Health, Tromsø, Norway, 2021a.

AMAP: Arctic Climate Change Update 2021: Key Trends and Impacts. Summary for Policy-makers, Tromsø, Norway, 2021b.

Andreae, M. O., Anderson, B. E., Blake, D. R., Bradshaw, J. D., Collins, J. E., Gregory, G. L., Sachse, G. W., and Shipham, M. C.: Influence of plumes from biomass burning on atmospheric chemistry over the equatorial and tropical South Atlantic during CITE 3, Journal of Geophysical Research: Atmospheres, 99, 12793–12808, https://doi.org/10.1029/94JD00263, 1994.

Angot, H., Blomquist, B., Howard, D., Archer, S., Bariteau, L., Beck, I., Boyer, M., Crotwell, M., Helmig, D., Hueber, J., Jacobi, H.-W., Jokinen, T., Kulmala, M., Lan, X., Laurila, T., Madronich, M., Neff, D., Petäjä, T., Posman, K., Quéléver, L., Shupe, M. D., Vimont, I., and Schmale, J.: Year-round trace gas measurements in the central Arctic during the MOSAiC expedition, Sci Data, 9, 723, https://doi.org/10.1038/s41597-022-01769-6, 2022.

Antokhina, O. Y., Antokhin, P. N., Belan, B. D., Gochakov, A. V., Martynova, Y. V., Pustovalov, K. N., Tarabukina, L. D., and Devyatova, E. V.: Effects of Rossby Waves Breaking and Atmospheric Blocking Formation on the Extreme Forest Fire and Floods in Eastern Siberia 2019, Fire, 6, 122, https://doi.org/10.3390/fire6030122, 2023.

Asmi, E., Backman, J., Servomaa, H., Virkkula, A., Gini, M. I., Eleftheriadis, K., Müller, T., Ohata, S., Kondo, Y., and Hyvärinen, A.: Absorption instruments inter-comparison campaign at the Arctic Pallas station, Atmospheric Measurement Techniques, 14, 5397–5413, https://doi.org/10.5194/amt-14-5397-2021, 2021.

Bey, I., Jacob, D. J., Yantosca, R. M., Logan, J. A., Field, B. D., Fiore, A. M., Li, Q., Liu, H. Y., Mickley, L. J., and Schultz, M. G.: Global modeling of tropospheric chemistry with assimilated meteorology: Model description and evaluation, Journal of Geophysical Research: Atmospheres, 106, 23073–23095, https://doi.org/10.1029/2001JD000807, 2001.

Bhatt, U. S., Lader, R. T., Walsh, J. E., Bieniek, P. A., Thoman, R., Berman, M., Borries-Strigle, C., Bulock, K., Chriest, J., Hahn, M., Hendricks, A. S., Jandt, R., Little, J., McEvoy, D., Moore, C., Rupp, T. S., Schmidt, J., Stevens, E., Strader, H., Waigl, C., White, J., York, A., and Ziel, R.: Emerging

https://doi.org/10.5194/egusphere-2023-2315
Preprint. Discussion started: 26 October 2023

Anthropogenic Influences on the Southcentral Alaska Temperature and Precipitation Extremes and Related Fires in 2019, Land, 10, 82, https://doi.org/10.3390/land10010082, 2021.

Boyer, M., Aliaga, D., Pernov, J. B., Angot, H., Quelever, L. L. J., Dada, L., Heutte, B., Dall'Osto, M., Beddows, D. C. S., Brasseur, Z., Beck, I., Bucci, S., Duetsch, M., Stohl, A., Laurila, T., Asmi, E., Massling, A., Thomas, D. C., Nojgaard, J. K., Chan, T., Sharma, S., Tunved, P., Krejci, R., Hansson, H. C., Bianchi, F., Lehtipalo, K., Wiedensohler, A., Weinhold, K., Kulmala, M., Petaja, T., Sipila, M., Schmale, J., and Jokinen, T.: A full year of aerosol size distribution data from the central Arctic under an extreme positive Arctic Oscillation: insights from the Multidisciplinarydrifting Observatory for the Study of Arctic Climate (MOSAiC) expedition, Atmospheric Chemistry and Physics, 23, 389–415, https://doi.org/10.5194/acp-23-389-2023, 2023.

Chen, X., Kang, S., Hu, Y., and Yang, J.: Temporal and spatial analysis of vegetation fire activity in the circum-Arctic during 2001–2020, Research in Cold and Arid Regions, 15, 48–56, https://doi.org/10.1016/j.rcar.2023.03.002, 2023.

Chin, M., Jacob, D. J., Munger, J. W., Parrish, D. D., and Doddridge, B. G.: Relationship of ozone and carbon monoxide over North America, Journal of Geophysical Research: Atmospheres, 99, 14565–14573, https://doi.org/10.1029/94JD00907, 1994.

Dall'Osto, M., Park, J., Kim, J. H., Kang, S. H., Park, K., Beddows, D. C. S., Harrison, R. M., and Yoon, Y. J.: Arctic ship-based evidence of new particle formation events in the Chukchi and East Siberian Seas, Atmospheric Environment, 223, https://doi.org/10.1016/j.atmosenv.2019.117232, 2020.

Ding, M. H., Tian, B., Zhang, T., Tang, J., Peng, H., Bian, L. G., and Sun, W. J.: Shipborne observations of atmospheric black carbon aerosol from Shanghai to the Arctic Ocean during the 7th Chinese Arctic Research Expedition, Atmospheric Research, 210, 34–40, https://doi.org/10.1016/j.atmosres.2018.04.016, 2018.

Drinovec, L., Močnik, G., Zotter, P., Prévôt, A. S. H., Ruckstuhl, C., Coz, E., Rupakheti, M., Sciare, J., Müller, T., Wiedensohler, A., and Hansen, A. D. A.: The "dual-spot" Aethalometer: an improved measurement of aerosol black carbon with real-time loading compensation, Atmospheric Measurement Techniques, 8, 1965–1979, https://doi.org/10.5194/amt-8-1965-2015, 2015.

Hayasaka, H.: Fire Weather Conditions in Boreal and Polar Regions in 2002-2021, Atmosphere, 13, https://doi.org/10.3390/atmos13071117, 2022.

Ikeda, K., Tanimoto, H., Sugita, T., Akiyoshi, H., Kanaya, Y., Zhu, C. M., and Taketani, F.: Tagged tracer simulations of black carbon in the Arctic: transport, source contributions, and budget, Atmospheric Chemistry and Physics, 17, 10515–10533, https://doi.org/10.5194/acp-17-10515-2017, 2017.

Ikeda, K., Tanimoto, H., Kanaya, Y., and Taketani, F.: Evaluation of anthropogenic emissions of black carbon from East Asia in six inventories: constraints from model simulations and surface observations on Fukue Island, Japan, Environmental Science-Atmospheres, 2, 416–427, https://doi.org/10.1039/d1ea00051a, 2022.

IPCC: Climate Change 2021: The Physical Science Basis. Contribution of Working Group I to the Sixth Assessment Report of the Intergovernmental Panel on Climate Change, Cambridge, United Kingdom and New York, NY, USA, https://doi.org/10.1017/9781009157896, 2021.

https://doi.org/10.5194/egusphere-2023-2315
Preprint. Discussion started: 26 October 2023

Jurányi, Z., Zanatta, M., Lund, M. T., Samset, B. H., Skeie, R. B., Sharma, S., Wendisch, M., and Herber, A.: Atmospheric concentrations of black carbon are substantially higher in spring than summer in the Arctic, Commun Earth Environ, 4, 1–12, https://doi.org/10.1038/s43247-023-00749-x, 2023.

Kim, G., Cho, H. J., Seo, A., Kim, D., Gim, Y., Lee, B. Y., Yoon, Y. J., and Park, K.: Comparison of Hygroscopicity, Volatility, and Mixing State of Subnnicrometer Particles between Cruises over the Arctic Ocean and the Pacific Ocean, Environmental Science & Technology, 49, 12024–12035, https://doi.org/10.1021/acs.est.5b01505, 2015.

Klimont, Z., Kupiainen, K., Heyes, C., Purohit, P., Cofala, J., Rafaj, P., Borken-Kleefeld, J., and Schöpp, W.: Global anthropogenic emissions of particulate matter including black carbon, Atmospheric Chemistry and Physics, 17, 8681–8723, https://doi.org/10.5194/acp-17-8681-2017, 2017.

Laing, J. R., Jaffe, D. A., and Arthur J. Sedlacek, I. I. I.: Comparison of Filter-based Absorption Measurements of Biomass Burning Aerosol and Background Aerosol at the Mt. Bachelor Observatory, Aerosol Air Qual. Res., 20, 663–678, https://doi.org/10.4209/aaqr.2019.06.0298, 2020.

McCarty, J. L., Aalto, J., Paunu, V.-V., Arnold, S. R., Eckhardt, S., Klimont, Z., Fain, J. J., Evangeliou, N., Venäläinen, A., Tchebakova, N. M., Parfenova, E. I., Kupiainen, K., Soja, A. J., Huang, L., and Wilson, S.: Reviews and syntheses: Arctic fire regimes and emissions in the 21st century, Biogeosciences, 18, 5053–5083, https://doi.org/10.5194/bg-18-5053-2021, 2021.

McFarquhar, G. M., Ghan, S., Verlinde, J., Korolev, A., Strapp, J. W., Schmid, B., Tomlinson, J. M., Wolde, M., Brooks, S. D., Cziczo, D., Dubey, M. K., Fan, J. W., Flynn, C., Gultepe, I., Hubbe, J., Gilles, M. K., Laskin, A., Lawson, P., Leaitch, W. R., Liu, P., Liu, X. H., Lubin, D., Mazzoleni, C., Macdonald, A. M., Moffet, R. C., Morrison, H., Ovchinnikov, M., Shupe, M. D., Turner, D. D., Xie, S. C., Zelenyuk, A., Bae, K., Freer, M., and Glen, A.: INDIRECT AND SEMI-DIRECT AEROSOL CAMPAIGN The Impact of Arctic Aerosols on Clouds, Bulletin of the American Meteorological Society, 92, 183–201, https://doi.org/10.1175/2010bams2935.1, 2011.

Moteki, N. and Kondo, Y.: Dependence of Laser-Induced Incandescence on Physical Properties of Black Carbon Aerosols: Measurements and Theoretical Interpretation, Aerosol Science and Technology, 44, 663–675, https://doi.org/10.1080/02786826.2010.484450, 2010.

Nagovitsyna, E. S., Poddubny, V. A., Karasev, A. A., Kabanov, D. M., Sidorova, O. R., and Maslovsky, A. S.: Assessment of the Spatial Structure of Black Carbon Concentrations in the Near-Surface Arctic Atmosphere, Atmosphere, 14, https://doi.org/10.3390/atmos14010139, 2023.

Ohata, S., Kondo, Y., Moteki, N., Mori, T., Yoshida, A., Sinha, P. R., and Koike, M.: Accuracy of black carbon measurements by a filter-based absorption photometer with a heated inlet, Aerosol Science and Technology, 53, 1079–1091, https://doi.org/10.1080/02786826.2019.1627283, 2019.

Ohata, S., Koike, M., Yoshida, A., Moteki, N., Adachi, K., Oshima, N., Matsui, H., Eppers, O., Bozem, H., Zanatta, M., and Herber, A. B.: Arctic black carbon during PAMARCMiP 2018 and previous aircraft experiments in spring, Atmospheric Chemistry and Physics, 21, 15861–15881, https://doi.org/10.5194/acp-21-15861-2021, 2021a.

Ohata, Sho, Mori, Tatsuhiro, Kondo, Yutaka, Sharma, Sangeeta, Hyvarinen, Antti, Andrews, Elisabeth, Tunved, Peter, Asmi, Eija, Backman, John, Servomaa, Henri, Veber, Daniel, Eleftheriadis, Konstantinos, Vratolis, Stergios, Krejci, Radovan, Zieger, Paul, Koike, Makoto, Kanaya, Yugo, Yoshida, Atsuhi, Moteki, Nobuhiro, Zhao, Yongjing, Tobo, Yutaka, Matsushita, Junji, and Oshima, Naga: Black carbon

https://doi.org/10.5194/egusphere-2023-2315
Preprint. Discussion started: 26 October 2023

mass concentrations and aerosol light absorption coefficients measured at Arctic sites (1.01), https://doi.org/10.17592/001.2020112001, 2021b.

Oshima, N., Yukimoto, S., Deushi, M., Koshiro, T., Kawai, H., Tanaka, T. Y., and Yoshida, K.: Global and Arctic effective radiative forcing of anthropogenic gases and aerosols in MRI-ESM2.0, Progress in Earth and Planetary Science, 7, https://doi.org/10.1186/s40645-020-00348-w, 2020.

Pan, X., Ichoku, C., Chin, M., Bian, H., Darmenov, A., Colarco, P., Ellison, L., Kucsera, T., da Silva, A., Wang, J., Oda, T., and Cui, G.: Six global biomass burning emission datasets: intercomparison and application in one global aerosol model, Atmospheric Chemistry and Physics, 20, 969–994, https://doi.org/10.5194/acp-20-969-2020, 2020.

Pankratova, N. V., Belikov, I. B., Belousov, V. A., Kopeikin, V. M., Skorokhod, A. I., Shtabkin, Y. A., Malafeev, G. V., and Flint, M. V.: Concentration and Isotopic Composition of Methane, Associated Gases, and Black Carbon over Russian Arctic Seas (Shipborne Measurements), Oceanology, 60, 593–602, https://doi.org/10.1134/s0001437020050197, 2020.

Paris, J.-D., Stohl, A., Ciais, P., Nédélec, P., Belan, B. D., Arshinov, M. Y., and Ramonet, M.: Source-receptor relationships for airborne measurements of CO2, CO and O3 above Siberia: a cluster-based approach, Atmospheric Chemistry and Physics, 10, 1671–1687, https://doi.org/10.5194/acp-10-1671-2010, 2010.

Park, J., Dall'Osto, M., Park, K., Gim, Y., Kang, H. J., Jang, E., Park, K.-T., Park, M., Yum, S. S., Jung, J., Lee, B. Y., and Yoon, Y. J.: Shipborne observations reveal contrasting Arctic marine, Arctic terrestrial and Pacific marine aerosol properties, Atmospheric Chemistry and Physics, 20, 5573–5590, https://doi.org/10.5194/acp-20-5573-2020, 2020.

Petzold, A., Ogren, J. A., Fiebig, M., Laj, P., Li, S. M., Baltensperger, U., Holzer-Popp, T., Kinne, S., Pappalardo, G., Sugimoto, N., Wehrli, C., Wiedensohler, A., and Zhang, X. Y.: Recommendations for reporting "black carbon" measurements, Atmospheric Chemistry and Physics, 13, 8365–8379, https://doi.org/10.5194/acp-13-8365-2013, 2013.

Pfannerstill, E. Y., Wang, N., Edtbauer, A., Bourtsoukidis, E., Crowley, J. N., Dienhart, D., Eger, P. G., Ernle, L., Fischer, H., Hottmann, B., Paris, J.-D., Stönner, C., Tadic, I., Walter, D., Lelieveld, J., and Williams, J.: Shipborne measurements of total OH reactivity around the Arabian Peninsula and its role in ozone chemistry, Atmospheric Chemistry and Physics, 19, 11501–11523, https://doi.org/10.5194/acp-19-11501-2019, 2019.

Popovicheva, O. B., Evangeliou, N., Eleftheriadis, K., Kalogridis, A. C., Sitnikov, N., Eckhardt, S., and Stohl, A.: Black Carbon Sources Constrained by Observations in the Russian High Arctic, Environmental Science & Technology, 51, 3871–3879, https://doi.org/10.1021/acs.est.6b05832, 2017.

Popovicheva, O. B., Evangeliou, N., Kobelev, V. O., Chichaeva, M. A., Eleftheriadis, K., Gregorič, A., and Kasimov, N. S.: Siberian Arctic black carbon: gas flaring and wildfire impact, Atmospheric Chemistry and Physics, 22, 5983–6000, https://doi.org/10.5194/acp-22-5983-2022, 2022.

Sakerin, S. M., Bobrikov, A. A., Bukin, O. A., Golobokova, L. P., Pol'kin, V. V., Shmirko, K. A., Kabanov, D. M., Khodzher, T. V., Onischuk, N. A., Pavlov, A. N., Potemkin, V. L., and Radionov, V. F.: On measurements of aerosol-gas composition of the atmosphere during two expeditions in 2013 along the Northern Sea Route, Atmospheric Chemistry and Physics, 15, 12413–12443, https://doi.org/10.5194/acp-15-12413-2015, 2015.

https://doi.org/10.5194/egusphere-2023-2315
Preprint. Discussion started: 26 October 2023

Sakerin, S. M., Kabanov, D. M., Makarov, V. I., Pol'kin, V. V., Popova, S. A., Chankina, O. V., Pochufarov, A. O., Radionov, V. E., and Rize, D. D.: Spatial Distribution of Atmospheric Aerosol Physicochemical Characteristics in the Russian Sector of the Arctic Ocean, Atmosphere, 11, https://doi.org/10.3390/atmos11111170, 2020.

Sakerin, S. M., Kabanov, D. M., Kopeikin, V. M., Kruglinsky, I. A., Novigatsky, A. N., Pol'kin, V. V., Shevchenko, V. P., and Turchinovich, Y. S.: Spatial Distribution of Black Carbon Concentrations in the Atmosphere of the North Atlantic and the European Sector of the Arctic Ocean, Atmosphere, 12, https://doi.org/10.3390/atmos12080949, 2021.

Sasakawa, M., Machida, T., Tsuda, N., Arshinov, M., Davydov, D., Fofonov, A., and Krasnov, O.: Aircraft and tower measurements of CO2 concentration in the planetary boundary layer and the lower free troposphere over southern taiga in West Siberia: Long-term records from 2002 to 2011, Journal of Geophysical Research: Atmospheres, 118, 9489–9498, https://doi.org/10.1002/jgrd.50755, 2013.

Schmale, J., Sharma, S., Decesari, S., Pernov, J., Massling, A., Hansson, H. C., von Salzen, K., Skov, H., Andrews, E., Quinn, P. K., Upchurch, L. M., Eleftheriadis, K., Traversi, R., Gilardoni, S., Mazzola, M., Laing, J., and Hopke, P.: Pan-Arctic seasonal cycles and long-term trends of aerosol properties from 10 observatories, Atmospheric Chemistry and Physics, 22, 3067–3096, https://doi.org/10.5194/acp-22-3067-2022, 2022.

Schulz, H., Zanatta, M., Bozem, H., Leaitch, W. R., Herber, A. B., Burkart, J., Willis, M. D., Kunkel, D., Hoor, P. M., Abbatt, J. P. D., and Gerdes, R.: High Arctic aircraft measurements characterising black carbon vertical variability in spring and summer, Atmospheric Chemistry and Physics, 19, 2361–2384, https://doi.org/10.5194/acp-19-2361-2019, 2019.

Shevchenko, V. P., Kopeikin, V. M., Novigatsky, A. N., and Malafeev, G. V.: Black Carbon in the Atmospheric Boundary Layer Over the North Atlantic and the Russian Arctic Seas in June-September 2017, Oceanology, 59, 692–696, https://doi.org/10.1134/s0001437019050199, 2019.

Sierau, B., Chang, R. Y. W., Leck, C., Paatero, J., and Lohmann, U.: Single-particle characterization of the high-Arctic summertime aerosol, Atmospheric Chemistry and Physics, 14, 7409–7430, https://doi.org/10.5194/acp-14-7409-2014, 2014.

Stein, A. F., Draxler, R. R., Rolph, G. D., Stunder, B. J. B., Cohen, M. D., and Ngan, F.: NOAA's HYSPLIT Atmospheric Transport and Dispersion Modeling System, Bulletin of the American Meteorological Society, 96, 2059–2077, https://doi.org/10.1175/BAMS-D-14-00110.1, 2015.

Stohl, A., Klimont, Z., Eckhardt, S., Kupiainen, K., Shevchenko, V. P., Kopeikin, V. M., and Novigatsky, A. N.: Black carbon in the Arctic: the underestimated role of gas flaring and residential combustion emissions, Atmospheric Chemistry and Physics, 13, 8833–8855, https://doi.org/10.5194/acp-13-8833-2013, 2013.

Taketani, F., Miyakawa, T., Takashima, H., Komazaki, Y., Pan, X., Kanaya, Y., and Inoue, J.: Shipborne observations of atmospheric black carbon aerosol particles over the Arctic Ocean, Bering Sea, and North Pacific Ocean during September 2014, Journal of Geophysical Research-Atmospheres, 121, 1914–1921, https://doi.org/10.1002/2015jd023648, 2016.

Taketani, F., Miyakawa, T., Takigawa, M., Yamaguchi, M., Komazaki, Y., Mordovskoi, P., Takashima, H., Zhu, C. M., Nishino, S., Tohjima, Y., and Kanaya, Y.: Characteristics of atmospheric black carbon and other aerosol particles over the Arctic Ocean in early autumn 2016: Influence from biomass burning

https://doi.org/10.5194/egusphere-2023-2315
Preprint. Discussion started: 26 October 2023

as assessed with observed microphysical properties and model simulations, Science of the Total Environment, 848, https://doi.org/10.1016/j.scitotenv.2022.157671, 2022.

Tanimoto, H., Kajii, Y., Hirokawa, J., Akimoto, H., and Minko, N. P.: The atmospheric impact of boreal forest fires in far eastern Siberia on the seasonal variation of carbon monoxide: Observations at Rishiri, A northern remote island in Japan, Geophysical Research Letters, 27, 4073–4076, https://doi.org/10.1029/2000GL011914, 2000.

Terpugova, S. A., Zenkova, P. N., Kabanov, D. M., Pol'kin, V. V., Golobokova, L. P., Panchenko, M. V., Sakerin, S. M., Lisitzin, A. P., Shevchenko, V. P., Politova, N. V., Kozlov, V. S., Khodzher, T. V., Shmargunov, V. P., and Chernov, D. G.: Results of the Study of Aerosol Characteristics in the Atmosphere of the Kara and Barents Seas in Summer and Autumn 2016, Atmospheric and Oceanic Optics, 31, 507–518, https://doi.org/10.1134/s1024856018050172, 2018.

van der Werf, G. R., Randerson, J. T., Giglio, L., van Leeuwen, T. T., Chen, Y., Rogers, B. M., Mu, M., van Marle, M. J. E., Morton, D. C., Collatz, G. J., Yokelson, R. J., and Kasibhatla, P. S.: Global fire emissions estimates during 1997–2016, Earth System Science Data, 9, 697–720, https://doi.org/10.5194/essd-9-697-2017, 2017.

Voronova, O. S., Zima, A. L., Kladov, V. L., and Cherepanova, E. V.: Anomalous Wildfires in Siberia in Summer 2019, Izvestiya Atmospheric and Oceanic Physics, 56, 1042–1052, https://doi.org/10.1134/s000143382009025x, 2020.

Whaley, C. H., Mahmood, R., von Salzen, K., Winter, B., Eckhardt, S., Arnold, S., Beagley, S., Becagli, S., Chien, R. Y., Christensen, J., Damani, S. M., Dong, X. Y., Eleftheriadis, K., Evangeliou, N., Faluvegi, G., Flanner, M., Fu, J. S., Gauss, M., Giardi, F., Gong, W. M., Hjorth, J. L., Huang, L., Im, U., Kanaya, Y., Krishnan, S., Klimont, Z., Kuhn, T., Langner, J., Law, K. S., Marelle, L., Massling, A., Olivie, D., Onishi, T., Oshima, N., Peng, Y. R., Plummer, D. A., Popovicheva, O., Pozzoli, L., Raut, J. C., Sand, M., Saunders, L. N., Schmale, J., Sharma, S., Skeie, R. B., Skov, H., Taketani, F., Thomas, M. A., Traversi, R., Tsigaridis, K., Tsyro, S., Turnock, S., Vitale, V., Walker, K. A., Wang, M. Q., Watson-Parris, D., and Weiss-Gibbons, T.: Model evaluation of short-lived climate forcers for the Arctic Monitoring and Assessment Programme: a multi-species, multi-model study, Atmospheric Chemistry and Physics, 22, 5775–5828, https://doi.org/10.5194/acp-22-5775-2022, 2022.

Xie, Z. Q., Blum, J. D., Utsunomiya, S., Ewing, R. C., Wang, X. M., and Sun, L. G.: Summertime carbonaceous aerosols collected in the marine boundary layer of the Arctic Ocean, Journal of Geophysical Research-Atmospheres, 112, https://doi.org/10.1029/2006jd007247, 2007.

Zhu, C. M., Kanaya, Y., Takigawa, M., Ikeda, K., Tanimoto, H., Taketani, F., Miyakawa, T., Kobayashi, H., and Pisso, I.: FLEXPART v10.1 simulation of source contributions to Arctic black carbon, Atmospheric Chemistry and Physics, 20, 1641–1656, https://doi.org/10.5194/acp-20-1641-2020, 2020.